Int. J. Radiation Oncology Biol. Phys., Vol. 47, No. 3, pp. 551–560, 2000

0360-3016/00/$–see front matter

ELSEVIER

PII S0360-3016(00)00467-3

**CRITICAL REVIEW**

# TOWARDS MULTIDIMENSIONAL RADIOTHERAPY (MD-CRT): BIOLOGICAL IMAGING AND BIOLOGICAL CONFORMALITY

C. CLIFTON LING, PH.D.,* JOHN HUMM, PH.D.,* STEVEN LARSON, M.D.,† HOWARD AMOLS, PH.D.,* ZVI FUKS, M.D.,‡ STEVEN LEIBEL, M.D.,‡ AND JASON A. KOUTCHER, M.D., PH.D.*

Departments of *Medical Physics, †Radiology, and ‡Radiation Oncology, Memorial Sloan Kettering Cancer Center, New York, NY

**Purpose: The goals of this study were to survey and summarize the advances in imaging that have potential applications in radiation oncology, and to explore the concept of integrating physical and biological conformality in multidimensional conformal radiotherapy (MD-CRT).**

**Methods and Materials: The advances in three-dimensional conformal radiotherapy (3D-CRT) have greatly improved the physical conformality of treatment planning and delivery. The development of intensity-modulated radiotherapy (IMRT) has provided the "dose painting" or "dose sculpting" ability to further customize the delivered dose distribution. The improved capabilities of nuclear magnetic resonance imaging and spectroscopy, and of positron emission tomography, are beginning to provide physiological and functional information about the tumor and its surroundings. In addition, molecular imaging promises to reveal tumor biology at the genotype and phenotype level. These developments converge to provide significant opportunities for enhancing the success of radiotherapy.**

**Results: The ability of IMRT to deliver nonuniform dose patterns by design brings to fore the question of how to "dose paint" and "dose sculpt", leading to the suggestion that "biological" images may be of assistance. In contrast to the conventional radiological images that primarily provide anatomical information, biological images reveal metabolic, functional, physiological, genotypic, and phenotypic data. Important for radiotherapy, the new and noninvasive imaging methods may yield three-dimensional radiobiological information. Studies are urgently needed to identify genotypes and phenotypes that affect radiosensitivity, and to devise methods to image them noninvasively. Incremental to the concept of gross, clinical, and planning target volumes (GTV, CTV, and PTV), we propose the concept of "biological target volume" (BTV) and hypothesize that BTV can be derived from biological images and that their use may incrementally improve target delineation and dose delivery. We emphasize, however, that much basic research and clinical studies are needed before this potential can be realized.**

**Conclusions: Whereas IMRT may have initiated the beginning of the end relative to physical conformality in radiotherapy, biological imaging may launch the beginning of a new era of biological conformality. In combination, these approaches constitute MD-CRT that may further improve the efficacy of cancer radiotherapy in the new millennium.** **© 2000 Elsevier Science Inc.**

**Biological imaging, Conformal radiotherapy.**

## INTRODUCTION

Radiological images have played an important role in medicine since the discovery of X-rays by Roentgen in 1896. In the last two decades, the advent of computed tomography (CT) and magnetic resonance imaging (MRI) has brought a quantum leap to our ability to visualize the human anatomy. Indeed, these advances have directly and significantly improved cancer diagnosis and treatment. In addition, advances in nuclear medicine imaging, with the widespread implementation of single photon emission computed tomography (SPECT) and the emerging widespread availability of positron emission tomography (PET), hold tremendous promise for improving the management of human cancer.

Recent developments in cancer detection, diagnosis, and treatment have suggested new types of images and intensified our need for them. This realization evolved with improvements in imaging and radiotherapy treatment technology, the spectacular advance in our knowledge of cancer at the molecular level, and the cross-fertilization of the multiple disciplines. Whereas up to the present, radiological images are largely anatomical, the new types of images can provide biological and mechanistic data, for example, metabolic information from PET scanning with fluorodeoxyglucose (FDG) radiolabeled with $^{18}$F and functional/meta-

Reprint requests to: C. Clifton Ling, Department of Radiation Oncology, Memorial Sloan-Kettering Cancer Center, 1275 York Ave., New York, NY 10021. E-mail: lingc@mskcc.org

*Acknowledgment*—Supported in part by Grant CA 59017 from the National Cancer Institute, Department of Health and Human Services, Bethesda, Maryland.

Accepted for publication 19 November 1999.

bolic data from nuclear magnetic resonance imaging and spectroscopy (MRI/MRS) studies. Under development are potential methods to characterize the genotype and phenotype of tumors by noninvasive molecular imaging (1–4).

Given the wide spectrum of information that the "new" imaging techniques can unfold, we suggest the descriptor "biological" for this class of images (in contrast to anatomical). Biological images broadly include those in the metabolic, biochemical, physiological, and functional categories, and they should also encompass molecular, genotypic, and phenotypic images presently under investigation. For radiation therapy, images that give information about factors (e.g., tumor hypoxia, $T_{pot}$) that influence radiosensitivity and treatment outcome can be regarded as radiobiological images.

Biological images are needed and useful for many reasons. Images that yield genotype and phenotype information would be helpful for genetic and molecular diagnosis, and for gene therapy. MR functional imaging of the brain may help surgical and other forms of local–regional therapy to avoid critical neurological structures (5). In radiotherapy, the advent of three-dimensional conformal radiotherapy (3D-CRT) and intensity-modulated radiotherapy (IMRT) has escalated the need for images, and in particular biological images, as will be discussed (6, 7).

In the last half of this (soon to become past) century, a number of major technological advances have significantly impacted upon the practice of radiotherapy and incrementally improved its therapeutic efficacy. These include the Co-60 teletherapy unit, medical linear accelerators, treatment simulators, afterloading and remote afterloading techniques, radium and radon substitutes, and computerized treatment planning. In the last decade, patient-specific 3D images are increasingly applied to treatment planning, 3D-CRT planning systems are maturing and becoming widely available, computer-controlled systems and multileaf collimators are emerging as standard features in medical linear accelerators, and the use of electronic portal imaging devices is gradually becoming established. Most recently, the new buzz words are inverse planning and IMRT, advances that have the potential of delivering exquisitely conformal dose distributions to the treatment target relative to the dose-limiting normal structures (6, 7).

At Memorial Sloan-Kettering Cancer Center (MSKCC), inverse planning and IMRT with dynamic multileaf collimators have been clinically implemented since October 1995 (6–11). Initially, the inverse planning algorithm was that of Bortfeld, adapted and incorporated into the Memorial Sloan-Kettering Treatment Planning System (8, 9). More recently, the method of Spirou and Chui has been applied clinically (10, 11). In their approach, the conjugate gradient method is applied to minimize an objective function that is basically the deviation from the desired dose in the various structures of interest (10). Depending on the specific structure, the associated objective function can be cast as a hard constraint, a soft constraint, or a dose–volume constraint. As of the fall of 1999, over 600 patients with cancers of the prostate, head/neck, and breast have been treated with IMRT at MSKCC. Operationally, the modality is well-accepted. In terms of radiation dose, our experience indicates a precision of about 1%. Although the potential clinical benefits associated with the increased dose conformality must be evaluated in outcome studies, preliminary results in terms of reducing treatment-related morbidity and increasing local control appear promising.

Indeed, current technology for delivering conformally shaped external beam radiation therapy may have exceeded our ability to localize tumors and normal tissues by conventional imaging techniques. In particular, IMRT can produce isodose distributions capable of delivering different dose prescriptions to multiple target sites with extremely high dose gradients between tumor and normal tissues. Consider, for example, Fig. 1 which demonstrates an ultraconformal external beam treatment of the prostate. In this example, we assume that biological imaging techniques exist which permit localization of regions within the prostate that contain highest tumor burden (gross target volume [GTV], outlined in orange), and also identification of urethra (blue outline) and prostatic capsule (planning target volume [PTV], green outline). We show in Fig. 1 the exquisite capability, using the existing MSKCC inverse treatment planning system, to sculpt the dose to the desired shape. An analysis of the associated dose–volume histograms (DVHs) demonstrates that the goals of the treatment design are well met: namely, to deliver 99 Gy to the GTV, 91 Gy to the PTV, no more than 86 Gy to urethra, and no more than 76 Gy to no more than 30% of the rectal wall. This treatment plan is currently achievable using a 10-field IMRT treatment technique with 15 MV photons.

The ability of IMRT to "paint" (in 2D) or "sculpt" (in 3D) the dose, and to produce exquisitely conformal dose distributions within the constraints of radiation propagation and scatter, begs the "64 million dollar question" as to how to paint or sculpt. Our hypothesis is that noninvasive biological imaging may provide the pertinent information to guide the painting or sculpting of the optimal dose distribution. There has been much laboratory and clinical research on the so-called predictive assays, i.e., the use of radiobiological characteristics such as proliferative activity (potential doubling time [$T_{pot}$]), radiosensitivity (the surviving fraction at a dose of 2 Gy [$SF_2$]), energy status (relative to sublethal damage repair), pH (a possible surrogate of hypoxia), tumor hypoxia, etc. as prognosticators of radiation treatment outcome (12). Noninvasive biological imaging is an incremental advance in the same direction and may provide "radiobiological phenotypes" (in the nomenclature of the "new" biology) of individual tumors. Important for IMRT, the spatial (geometrical) distribution of the radiobiological phenotypes is also provided by such images, based on which dose distribution may be designed conforming to both the physical (geometrical) and the biological attributes.

Given the above, the purpose of this report is to give an overview of the development of the various forms of biological imaging in the context of the needs of radiotherapy.

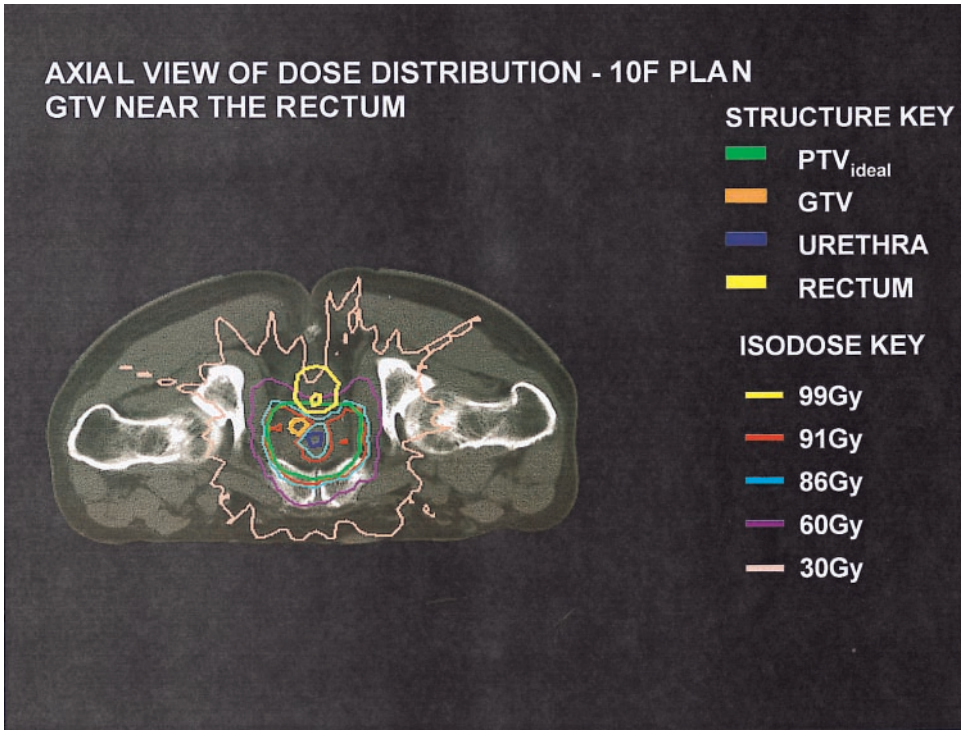


Fig. 1. An example of an ultraconformal, or "dose painted" external beam treatment of the prostate. We assume that biological imaging techniques exist which permit localization of regions within the prostate that contain highest tumor burden (GTV, outlined in orange), and also identification of urethra (blue outline) and prostatic capsule (PTV, green outline). This 10-field plan demonstrates the exquisite capability, using the existing MSKCC inverse treatment planning system, to sculpt the dose to the desired shape.

These advances will be grouped into three categories: MRI/MRS, biological imaging with PET, and molecular imaging/radiobiological phenotyping. (Given that some of these approaches are in early development stage and others in preclinical or clinical testing, it is neither our intent nor possible to give a detailed review and comparison of the relative merits of the different options.) Following these discussions, we introduce the concept of biological target volume (BTV) based on biological imaging, thus integrating physical and biological conformality and leading to multidimensional conformal radiotherapy (MD-CRT).

## MAGNETIC RESONANCE IMAGING AND SPECTROSCOPY

The excellent soft tissue contrast, based on differences in the T1 and T2 relaxation parameters of normal and pathologic states, underlies the significant utility of MRI in cancer detection and staging. However, the early promise, based on findings that malignant tissues have higher T1 and T2 values than normal tissue, has been somewhat modulated due to inadequate specificity. Methods for contrast enhancement have been developed to provide images that also yield tumor physiological and microenvironmental information, such as blood flow (perfusion or diffusion), hypoxia, pH, etc. These parameters may be important prognosticators relative to tumor responsiveness to radiation and other antineoplastic treatment. In addition, it has been suggested that changes in these parameters can be monitored by magnetic resonance (13–15).

Tissue perfusion with submillimeter resolution can be estimated from the increase in the T1 signal after the bolus administration of a contrast agent such as gadolinium diethylenetriaminepenta-acetic acid (Gd-DTPA). With faster pulse sequences such as the echo-planar dynamic imaging (EPI) method, serial images at $<1$ second per frame can be obtained to track the uptake of the contrast agent. The derived parametric image can yield pixel by pixel information on blood volume, blood–brain barrier permeability, blood perfusion, diffusion, extravascular space, etc. The utility of such techniques to assess tumor grade and type, treatment efficacy, and possibly long-term prognosis as applied to brain, breast, sarcoma, and other sites is being studied.

For breast cancers, because benign lesions are less vascularized (16) than malignant ones, the use of dynamic contrast enhanced MRI to quantify vascularity may improve the specificity of detection (17). As tumor grade, metastatic potential, and neovascularity may be correlated (16, 18), dynamic MRI may also provide prognostic information (19).

Diffusion-weighted imaging (DWI), in measuring the mobility of water molecules and providing information on the media and/or barriers, may be used to distinguish normal

and pathological states (20). In its application of assessing treatment response of high-grade gliomas, the measured diffusion coefficients were used to differentiate between enhancing, nonenhancing, cystic, and necrotic regions (21). Applying this technique, Krabbe *et al.* studied 28 patients (12 with high-grade and 3 with low-grade gliomas, 7 with metastases, 5 with meningiomas, and 1 with a cerebral abscess) and reported that cerebral metastases could be distinguished from high-grade gliomas (22). Similarly, in 74 hepatic lesions (11 hemangiomas, 15 metastases, and 48 hepatocellular carcinomas), Ichikawa *et al.* reported distinguishable diffusion coefficients and suggested that this approach may be useful for differential diagnosis of these lesions and hepatocellular carcinomas from hemangiomas (23).

Advances in magnetic gradient technology and rapid imaging techniques have made possible the mapping of brain function (fMRI). One type of fMRI studies is based on the paramagnetic property of deoxygenated hemoglobin that induces local magnetic inhomogeneities, enhances the relaxation of the adjacent water molecules, and thereby decreases the T2 signal adjacent to the blood vessels. Task activation stimulates the brain, and increases blood flow and oxygen to the activated region, resulting in a higher oxyhemoglobin level and increased T2 signal. Such blood oxygenation level–dependent (BOLD) changes (24) have been observed during sensory stimulation, manual tasks, and a wide variety of other forms of activation (25, 26). An important application of this noninvasive procedure for surgical and radiation oncology is in conformal avoidance of critical areas of the brain to minimize the possibility of loss of critical functions (5, 27). The potential use of fMRI data for radiotherapy treatment planning with function-specific DVHs has been described by Hamilton *et al.* (5).

Nuclear magnetic resonance (NMR) spectroscopy is a powerful approach in that it can yield abundant biological information associated with many different biomolecules. Among the various techniques, proton ($^1$H) spectroscopy is attractive in terms of sensitivity, spatial resolution, signal to noise, and acquisition time. Molecules that can be studied with $^1$H spectroscopy include water, lipids (which are suppressed in most studies), choline, citrate, lactate, and creatine.

In the prostate, an elevated choline level (resulting from the enhanced phospholipid cell membrane turnover associated with tumor proliferation, increased cellularity, and growth) may be an indicator of active tumor. Recent studies from the University of California, San Francisco (UCSF) indicated that $^1$H-NMR may provide useful parametric images of prostate cancer for radiotherapy treatment design and for response assessment (28–31). Specifically, the tumor is higher in choline concentration (choline/citrate ratio of $2.1 \pm 1.3$) in contrast to the higher citrate level in normal prostatic tissue and benign hypertrophy (choline/citrate ratio of $0.61 \pm 0.21$) (28–31). Based on this information and patient-specific parametric images, the investigators at UCSF are conducting a clinical trial in which IMRT treatment plans are designed to deliver a higher dose to those regions with a higher than normal choline/citrate ratio.

Other studies have suggested that $^1$H-NMR can be used to monitor tumor response, although it remains to be seen whether they will reliably serve as an early indicator. For example, Wald *et al.* observed a correlation between choline reduction and response to brachytherapy in brain tumors, and found that rising choline level corresponded to tumor recurrence (32). Speck *et al.* were able to follow tumor response to brachytherapy and noted a decrease in choline due to necrosis (33). Tedeschi *et al.* studied tumor progression in 27 patients with gliomas and found that progressive disease was characterized by an increase in choline level of greater than 45% (34).

Other compounds that have been detected by $^1$H-NMR spectroscopy *in vivo* include creatine (indicative of energy metabolism), glutamate (a major excitatory neurotransmitter and energy source), myo-inositol (involved in intracellular signaling pathways related to growth), and gamma aminobutyric acid (a major inhibitory neurotransmitter). The molecule of lactate, detectable by $^1$H-NMR, is of particular interest. Lactate increases in direct relation to anaerobic glycolysis caused by tumor hypoxia, ischemia, or infection. As early as 1983, Behar *et al.* reported that lactate levels were correlated with hypoxia in the rat brain (35). Recent data have indicated that high tumor levels of lactate are associated with an adverse prognosis. Schwickert *et al.* studied 10 patients with cervical cancer and found that lactate levels were significantly higher in patients with metastatic spread compared to patients with localized disease (36). Similarly, Walenta *et al.* studied 15 patients with head and neck tumors and concluded that high levels of lactate are associated with metastatic disease (37). In a more recent study of 50 patients with laryngeal cancer, a similar prognostic relationship with tumor lactate levels was observed (Mark Dewhirst, personal communication, 2/99). Lactate has also been shown to change in response to radiation (38), suggesting that it may be involved in resistance to radiation.

NMR spectroscopy of $^{31}$P can provide information about tumor energy status (nucleoside triphosphates [NTP], phosphocreatine [PCr], inorganic phosphates [Pi], etc.), pH, and other biomolecules involved in the phosphorylation metabolic pathway. The membrane precursors phosphocholine (PC) and phosphoethanolamine (PE) have been resolved *in vivo* at high magnetic fields (14, 39, 40) and have been shown to change in response to radiation and chemotherapy. With $^1$H decoupling, PE and PC can be resolved with 1.5 T clinical magnets, and it has been suggested that they may be useful as an early predictor of tumor response. In a rodent model, PE increased and PC decreased in a dose-dependent manner, possibly due to changes in proliferation and growth fraction (41–43). Other investigators have observed that changes in energy (ATP/Pi) resulting from radiation and hyperthermia treatment correlated with the necrotic fraction in sarcoma at surgery and that $^{31}$P-NMR data correlated with hypoxia (43–46). Whether this information can serve

as a surrogate of tumor response to therapy remains to be defined.

## BIOLOGICAL IMAGING WITH PET

Whereas nuclear medicine approaches have long been useful in cancer diagnosis, the recent widespread availability of clinical PET scanners, and the adaptation of SPECT scanners for coincidence detection, have greatly enhanced the potential of radionuclide detection in cancer management. This method has the major advantages of being noninvasive, versatile (with the use of diverse biomolecules), and highly sensitive (capable of imaging concentrations as low as picomolar). Furthermore, the ability of such methods for quantitation of radioactivity uptake provides additional information on tumor characteristics that were previously unavailable.

The increased enthusiasm for PET scanning is in part due to the availability of FDG as a tracer. The increased glucose metabolism of cancer cells, as compared to normal tissues, underlies the enhanced uptake of FDG in malignant growth. Clinical studies of many disease sites, including brain, breast, head and neck, colorectal, and ovarian, have shown that PET imaging with FDG has the potential to improve the detection, staging, treatment design, and evaluation (47–51). It is most probable that FDG-PET will be increasingly useful and embraced as a tool for assessing human malignancy.

There have been a large number of clinical studies reporting the efficacy of FDG-PET in diagnosing and staging thoracic lesions, leading to the Health Care Financing Administration (HCFA) approval of reimbursement for PET studies in the thorax in 1997. Its use in clinical target volume (CTV) definition of cancer of the lung is only beginning to be explored. In a retrospective study, Kiffer *et al.* observed that coronal FDG-PET images would have influenced the radiation treatment field of 4 of 15 patients (52). In a prospective study, Munley *et al.* reported that PET data altered 34% (12 of 35) of treatment plans for their patients (53). Our preliminary data support these data on the ability of FDG-PET in detecting metabolic foci not detected on CT scans (Rosenzweig, personal communication).

The sensitivity of FDG-PET for detecting small lesions led to its exploratory use for outcome or recurrence assessment after radiotherapy of colorectal and head/neck tumors (54, 55). In the study involving 37 head/neck squamous cell carcinomas, the specific decrease in FDG uptake was correlated well with 3-year survival after radiotherapy (73% versus 22%) (55). In contrast, in 44 patients with colorectal cancer treated with combined photon and neutron therapy, only 50% showed decrease in FDG uptake despite good palliative results (54). In a patient with meningioma treated with radiation, Fischman reported no evidence of tumor but only reactive changes and necrosis in the surgical specimens from "hot" regions on the FDG-PET image (56). Other studies have also shown that, while the enhanced FDG-uptake in tumor is largely dependent upon the altered metabolism, there are other influential factors, including tumor burden, blood flow, tissue inflammation, cellular energy level, and hypoxia. Given the heterogeneous nature of human malignancy, it is possible that the usefulness of FDG-PET is disease-specific or even patient-specific. Clearly, an improved understanding of the effects of the above-mentioned factors will facilitate the interpretation of FDG-PET images in clinical situations.

Besides FDG, other PET tracers are beginning to be examined. A major class of compounds are the DNA precursors, either thymidine or deoxyuridine. These molecules, labeled with either $^{11}$C or $^{124}$I for PET or $^{131}$I for SPECT, are incorporated in DNA replication during the S phase of cycling cells and can be noninvasively imaged to identify regions of cell proliferation (57–59). Another group are the substrates for protein synthesis, e.g., $^{11}$C-labeled methionine or choline (60), with the latter being studied in prostate cancer since phosphatidylcholine is known to be elevated in that disease. Although none of these processes can be considered a direct measure of tumor aggressiveness or curability, each provides a measure of tumor characteristics that may be indirectly related to treatment outcome.

Another emerging PET application of potential importance is the detection of hypoxic cells, coincidental with the resurgent interest in tumor hypoxia. Since the observation of Thomlinson and Gray (61), tumor hypoxia has been regarded as an important reason for the failure of radiotherapy. Data for 6975 patients, accrued in 43 randomized trials using oxygen-mimicking sensitizers and hyperbaric oxygen, support the hypothesis that treatment outcome can be improved by reducing the influence of hypoxia (62). Recent clinical trials clearly demonstrated a correlation between hypoxia and radiocurability in both metastasis-containing lymph nodes in head and neck cancer and in cervical cancer (63, 64). Even among the patients who underwent surgery for cancer of the cervix, survival and relapse-free survival were poorer for those with hypoxic tumors (65). In high-grade soft tissue sarcomas, Brizel *et al.* reported an association between tumor hypoxia and the development of metastases following multimodality treatment (64). Thus, hypoxia may be associated with a more aggressive tumor phenotype, in addition to radioresistance. It follows that an assessment of tumor hypoxia may be of prognostic value, and important for making treatment decisions.

A spin-off of the search for hypoxic cell radiosensitizers is the finding that nitroimidazoles are preferentially and metabolically reduced in hypoxic cells (but not in aerobic ones), resulting in toxic bioreductive products that target hypoxic cells. Rasey *et al.* have demonstrated the efficacy of PET imaging with Fmiso (fluorinated misonidazole) in quantifying hypoxia in lung and head/neck cancers (66). In their study, 36 of the 37 tumors investigated had hypoxic regions, with fractional hypoxic volumes of 47% and 9% for non–small-cell lung and head/neck cancers, respectively (66). Chapman *et al.* have shown that SPECT with $^{131}$iodinated azomycine arabinocide ($^{131}$IAZA) can also detect tumor hypoxia in both small cell lung and head/neck

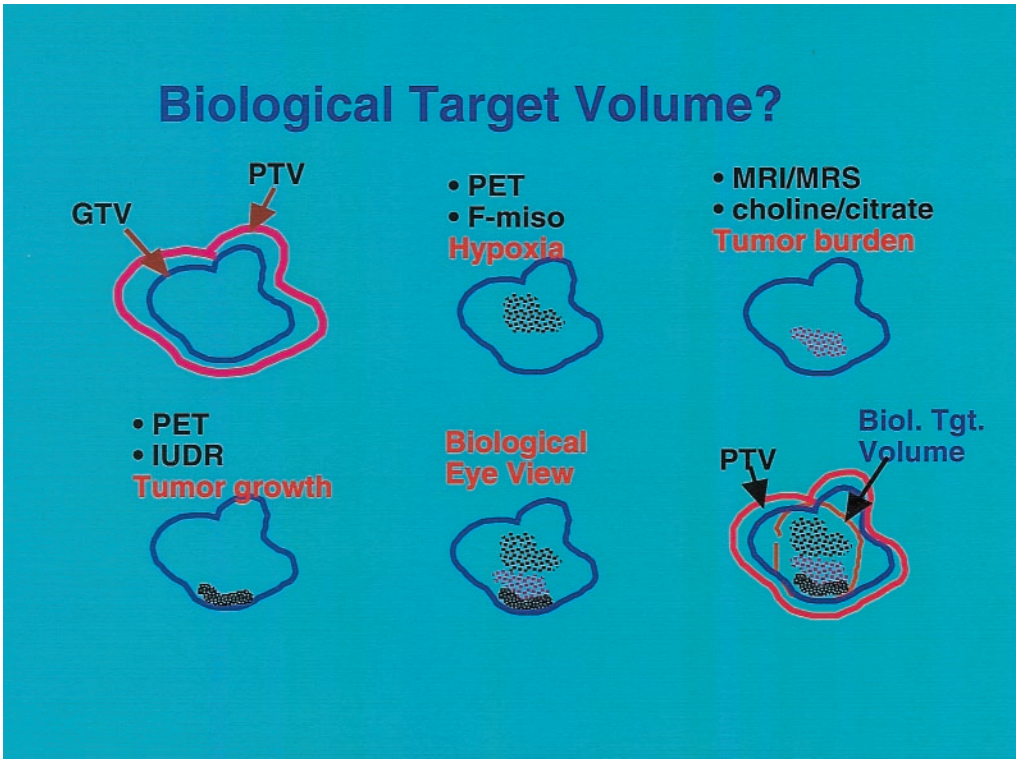


Fig. 2. An idealized schematic illustrating the concept of biological target volume (BTV). Whereas at present the target volume is characterized by the concepts of GTV, CTV, and PTV, biological images as depicted in Fig. 2 may provide information for defining the BTV to improve dose targeting to certain regions of the target volume. For example, regions of low $pO_2$ level may be derived from PET-$^{18}$F-misonidazole study, high tumor burden from MRI/MRS data of choline/citrate ratio, and high proliferation from PET-$^{124}$IUdR measurement.

cancers, despite the lower resolution of this imaging method (67). Motivated by these initial promising findings, but recognizing the inherent disadvantage of SPECT and the short half-life of $^{18}$F, research efforts are ongoing in our institution to explore PET radionuclides with longer half-lives to better match the 6–8 hr kinetics of tracer incorporation.

Several laboratories, including ours, are studying the potential of PET in detecting and imaging cell death, particularly as it relates to apoptosis. If imaging cell death *in vivo* is possible with PET scanning, we may have a noninvasive predictive assay that quantifies treatment-induced cell death, applicable to radiotherapy and other forms of cancer therapy. At present, annexin V is used in PET imaging of cell death. Annexin V is a 35–36 kDa calcium-dependent phospholipid-binding protein with a high affinity for phosphatidylserine (PS), located on the inner plasma membrane (and therefore inaccessible) in normal cells. During an early stage of apoptosis, the plasma membrane becomes depolarized, resulting in the translocation of PS to the outer surface where it becomes exposed to the extracellular milieu and accessible to annexin V. Recently, Blankenberg *et al.* and Vriens *et al.* have demonstrated in rodent models the detection of apoptosis with $^{99m}$Tc-labeled Annexin V, after coronary graft implants and in hepatic treatment with anti-FAS antibody, respectively (68, 69). Of significance, noninvasive images of apoptosis were obtained.

## MOLECULAR IMAGING AND RADIOBIOLOGICAL PHENOTYPING

The rapid advance of our understanding of human cancer at the molecular level and the intense interest to exploit such understanding in gene therapy have stimulated the development of noninvasive imaging methods to guide, monitor, and evaluate the efficacy of this form of cancer treatment. Both NMR and nuclear medicine approaches hold promise for noninvasive molecular imaging, although such methods are very much in infancy and developmental stages, and are primarily performed in preclinical studies.

Several strategies are generally employed for molecular imaging using NMR or nuclear medicine techniques. In the first approach, enzymatic processing of an agent and/or the metabolic trapping of a substrate would provide the image signal. For example, Tjuvajev *et al.* successfully monitored the *in vivo* transduction of the HSV1-tk marker gene using the $^{131}$I- or $^{124}$iodinated 2′Fluoro-1-D-arabinofuranosyl-5-iodo-uracil ($^{124}$I-FIAU) as the reporter substrate—with the level of metabolically trapped FIAU, detectable by SPECT or PET, representing the expression of the transduced gene (70). Similar but using NMR, Weissleder *et al.* were able to

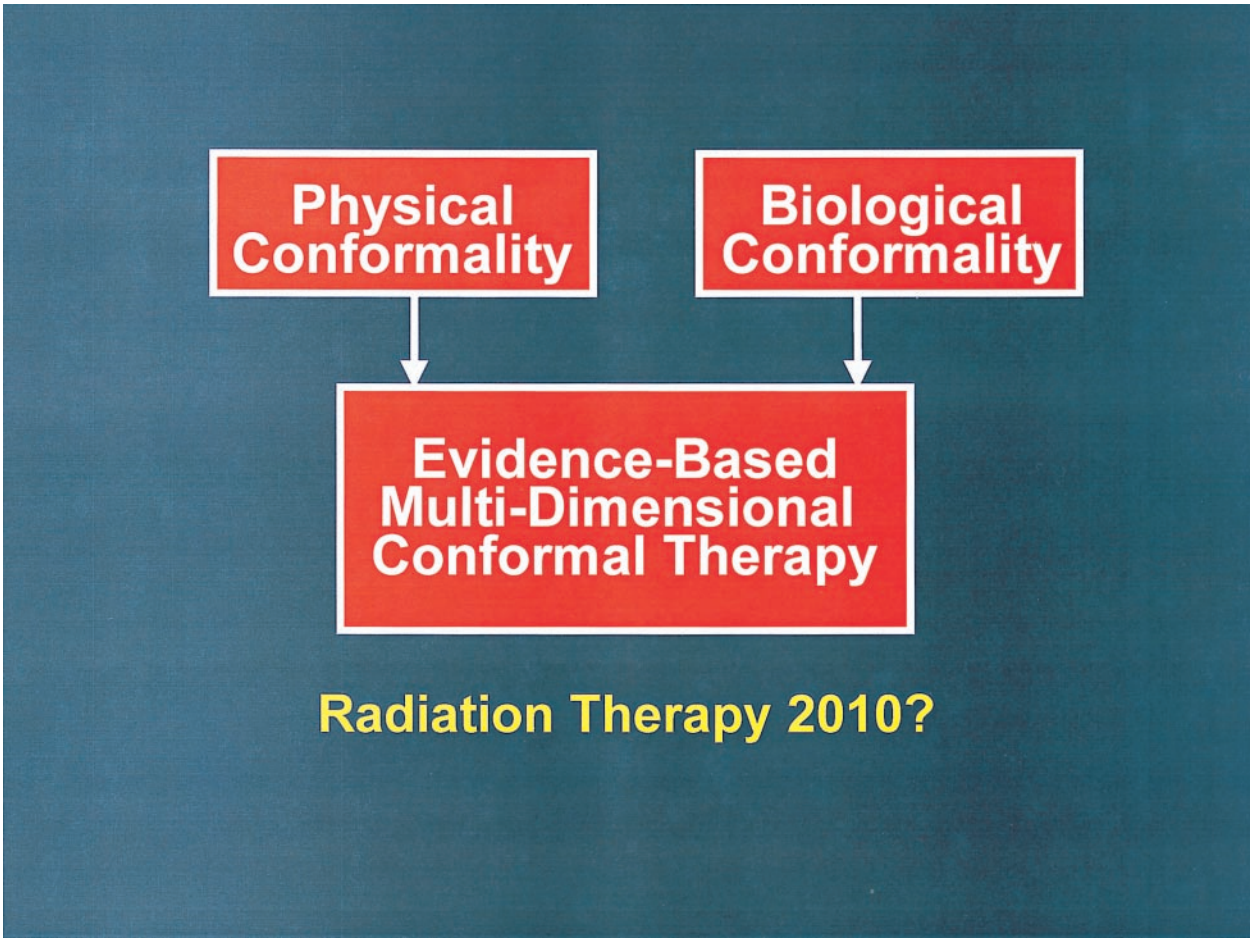


Fig. 3. MD-CRT combines the attributes of physical conformality of 3D-CRT, and the dose targeting ability of IMRT to conform the dose pattern to the radiobiological features of the target that may be derived from biological imaging.

ascertain the transfer (into *in vitro* cell culture) and expression of a vector coding for the human tyrosinase by imaging the enzymatic product melanin (3).

The second strategy targets cell surface receptors with imaging tracers. For example, Moore *et al.* showed that the expression and regulation of the human transferrin receptor (hTfR) can be visualized by NMR imaging using a novel probe with a sterically protected paramagnetic core (2, 71, 72). The same approach can be adopted using nuclear medicine detection techniques and radioactive tracers conjugated with receptor-specific ligands (71, 72). Another strategy for imaging gene expression is to use antisense molecules to target the relevant messenger RNA (mRNA) (4). This approach depends on a sufficient amount of target mRNA, accessibility of the binding domain, and the synthesis and stability of the marker antisense molecule (4).

Studies are urgently needed to explore and extend the above approaches for application to radiation oncology. Such efforts should be directed to at least two areas. The first is to identify genotypes and phenotypes that affect radiosensitivity, and the second is to devise methods to image them noninvasively. Whereas several genes (e.g., ATM, components of the DNA-PK, etc.) are well-known for their significant effects on DNA repair and radiosensitivity (73, 74), they do not account for the subtle variation in radiocurability encountered in clinical radiotherapy. Although there have been a number of studies examining the effects of gene expressions of myc, ras, p53, cyclins, etc. on radiosensitivity, to date no reliable correlation has been established (75–78). Nevertheless, endeavors to attempt radiobiological phenotyping need to be continued, in parallel with the more traditional and phenomenological predictive assays such as proliferative activity ($T_{pot}$), radiosensitivity ($SF_2$), and tumor hypoxia (12).

## GTV, CTV, PTV, BTV, AND MD-CRT

The concept of gross, clinical, and planning target volumes (GTV, CTV, and PTV), as proposed by the International Commission on Radiation Units and Measurements Report No. 50 (ICRU-50), is now well accepted and widely used in radiotherapy treatment design, especially for 3D-CRT (79). In general, cross-sectional images (CT and MRI) are used to delineate the GTV, CTV, and PTV, and radiation treatment portals are designed to entirely cover the PTV and deliver a uniform dose distribution to it.

The requirement for dose uniformity within the PTV in external beam treatment planning has been largely a matter

of tradition and convention. 3D-CRT and dose-escalation studies have stimulated discussion concerning this requirement in treatment design. Specifically, there have been suggestions that nonuniformity within the PTV, specifically regions of increased dose, may actually increase the local control. The ability of IMRT to deliver nonuniform dose patterns by design, brings to fore the question of how to "dose paint" and "dose sculpt." In this regard, we suggest that biological images may be of value. We emphasize, however, that much scientific research and clinical studies are needed before this potential can be realized.

A real-life example of using biological images for treatment planning and delivery is the work of the researchers at UCSF. As alluded to previously, they are evaluating the potential clinical gain of using IMRT to deliver a nonuniform dose distribution within the PTV, with a higher dose (than that prescribed) given to specific regions with active tumor. Such "dose sculpting" is guided by MRI/MRS images of choline/citrate ratio, taken as a surrogate for tumor burden. Another type of biological image is that of tumor hypoxia (66, 67, 80). If regions of low $pO_2$ within the tumor can be delineated using either PET or NMR, higher doses can be targeted specifically to the hypoxic fraction using IMRT. Likewise, if the signal intensity of FDG-PET can be correlated to tumor burden, IMRT treatment plan may be designed to optimize local control probability. Still another example would be the use of PET tracers (e.g., iodine-124-iododeoxyuridine $^{124}$IUdR) to image tumor repopulation during a course of radiotherapy so as to permit selectively delivering additional doses to those regions (57).

The schematics in Fig. 2 advance the concept of the "biological target volume" (BTV) and project a "blue-sky" scenario, combining the examples of biological images discussed above. We hypothesize that the BTV can be derived from biological images and that their use may guide customized dose delivery to the various parts of the treatment volume. As depicted in Fig. 2, regions of low $pO_2$ level (from PET-$^{18}$F-misonidazole study), high tumor burden (from MRI/MRS data of choline/citrate ratio), and high proliferation (from PET-$^{124}$IUdR measurement) may be considered *in toto* to design a BTV, based on which "dose painting" or "sculpting" strategy may be applied.

Whereas IMRT may have initiated the beginning of the end relative to the physical conformality of dose distribution in radiotherapy, biological imaging may launch the beginning of a new era of biological conformality. In combination, these approaches constitute MD-CRT that may further improve the efficacy of cancer radiotherapy in the new millennium (Fig. 3).

## REFERENCES


1. Kayyem JF, Kumar RM, Fraser SE, Meade TJ. Receptor-targeted co-transport of DNA and magnetic resonance contrast agents. *Chem Biol* 1995;2:615–620.
2. Moore A, Basilion JP, Chiocca EA, Weissleder R. Measuring transferrin receptor gene expression by NMR imaging. *Biochim Biophys Acta* 1998;1402:239–249.
3. Weissleder R, Simonova M, Bogdanova A, Bredow S, Enochs WS, Bogdanov A Jr. MR imaging and scintigraphy of gene expression through melanin induction. *Radiology* 1997;204: 425–429.
4. Urbain JL. Oncogenes, cancer and imaging. *J Nuclear Med* 1999;40:498–504.
5. Hamilton RJ, Sweeney PJ, Pelizzari CA, *et al.* Functional imaging in treatment planning of brain lesions. *Int J Radiat Oncol Biol Phys* 1997;37:181–188.
6. Ling CC, Burman C, Chui CS, *et al.* Conformal radiation treatment of prostate cancer using inversely-planned intensity-modulated photon beams produced with dynamic multileaf collimation [see comments]. *Int J Radiat Oncol Biol Phys* 1996;35:721–730.
7. Ling CC, Fuks Z. Conformal radiation treatment: A critical appraisal. *Eur J Cancer* 1995;5:799–803.
8. Bortfeld T, Burkelbach J, Boesecke R, Schlegel W. Methods of image reconstruction from projections applied to conformation radiotherapy. *Phys Med Biol* 1990;35:1423–1434.
9. Mohan R, Wang X, Jackson A, *et al.* The potential and limitations of the inverse radiotherapy technique. *Radiother Oncol* 1994;32:232–248.
10. Spirou SV, Chui CS. A gradient inverse planning algorithm with dose–volume constraints. *Med Phys* 1998;25:321–333.
11. Burman C, Chui CS, Kutcher G, *et al.* Planning, delivery, and quality assurance of intensity-modulated radiotherapy using dynamic multileaf collimator: A strategy for large-scale implementation for the treatment of carcinoma of the prostate. *Int J Radiat Oncol Biol Phys* 1997;39:863–873.
12. Bartelink H, Begg A, Coco Martin J, *et al.* Towards prediction and modulation of treatment response. *Radiother Oncol* 1999; 50:1–12.
13. Moon RB, Richards JH. Determination of intracellular pH by $^{31}$P magnetic resonance. *J Biol Chem* 1973;248:7276–7278.
14. Koutcher JA, Alfieri AA, Devitt ML, *et al.* Quantitative changes in tumor metabolism, partial pressure of oxygen, and radiobiological oxygenation status postradiation. *Cancer Res* 1992;52:4620–4627.
15. Okunieff P, Walsh CS, Vaupel P, *et al.* Effects of hydralazine on in vivo tumor energy metabolism, hematopoietic radiation sensitivity, and cardiovascular parameters. *Int J Radiat Oncol Biol Phys* 1989;16:1145–1148.
16. Weidner N, Semple JP, Welch WR, Folkman J. Tumor angiogenesis and metastasis: Correlation in invasive breast carcinoma. *N Engl J Med* 1991;324:1–8.
17. Kaiser WA, Zeitler E. MR imaging of the breast: Fast imaging sequences with and without Gd-DTPA. Preliminary observations. *Radiology* 1989;170(3 Pt 1):681–686.
18. Weidner N, Folkman J, Pozza F, *et al.* Tumor angiogenesis: A new significant and independent prognostic indicator in early-stage breast carcinoma [see comments]. *J Natl Cancer Inst* 1992;84:1875–1887.
19. Mussurakis S, Buckley DL, Horsman A. Dynamic MR imaging of invasive breast cancer: Correlation with tumour grade and other histological factors. *Br J Radiol* 1997;70:446–451.
20. Le Bihan D, Breton E, Lallemand D, Grenier P, Cabanis E, Laval-Jeantet M. MR imaging of intravoxel incoherent motions: Application to diffusion and perfusion in neurologic disorders. *Radiology* 1986;161:401–407.
21. Tien RD, Felsberg GJ, Friedman H, Brown M, MacFall J. MR imaging of high-grade cerebral gliomas: Value of diffusion-

weighted echoplanar pulse sequences. *AJR Am J Roentgenol* 1994;162:671–677.
22. Krabbe K, Gideon P, Wagn P, Hansen U, Thomsen C, Madsen F. MR diffusion imaging of human intracranial tumours. *Neuroradiology* 1997;39:483–489.
23. Ichikawa T, Haradome H, Hachiya J, Nitatori T, Araki T. Diffusion-weighted MR imaging with a single-shot echoplanar sequence: Detection and characterization of focal hepatic lesions. *AJR Am J Roentgenol* 1998;170:397–402.
24. Kim KH, Relkin NR, Lee KM, Hirsch J. Distinct cortical areas associated with native and second languages. *Nature* 1997; 388:171–174.
25. Belliveau JW, Kennedy DN Jr, McKinstry RC, *et al.* Functional mapping of the human visual cortex by magnetic resonance imaging. *Science* 1991;254:716–719.
26. Kim SG, Ashe J, Hendrich K, *et al.* Functional magnetic resonance imaging of motor cortex: Hemispheric asymmetry and handedness. *Science* 1993;261:615–617.
27. Fried I, Nenov VI, Ojemann SG, Woods RP. Functional MR and PET imaging of rolandic and visual cortices for neurosurgical planning. *J Neurosurg* 1995;83:854–861.
28. Kurhanewicz J, Vigneron DB, Hricak H, Narayan P, Carroll P, Nelson SJ. Three-dimensional H-1 MR spectroscopic imaging of the in situ human prostate with high (0.24–0.7-$cm^3$) spatial resolution. *Radiology* 1996;198:795–805.
29. Kaji Y, Kurhanewicz J, Hricak H, *et al.* Localizing prostate cancer in the presence of postbiopsy changes on MR images: Role of proton MR spectroscopic imaging. *Radiology* 1998; 206:785–790.
30. Kurhanewicz J, Vigneron DB, Hricak H, *et al.* Prostate cancer: Metabolic response to cryosurgery as detected with 3D H-1 MR spectroscopic imaging. *Radiology* 1996;200:489–496.
31. Parivar F, Hricak H, Shinohara K, *et al.* Detection of locally recurrent prostate cancer after cryosurgery: Evaluation by transrectal ultrasound, magnetic resonance imaging, and three-dimensional proton magnetic resonance spectroscopy. *Urology* 1996;48:594–599.
32. Wald LL, Nelson SJ, Day MR, *et al.* Serial proton magnetic resonance spectroscopy imaging of glioblastoma multiforme after brachytherapy. *J Neurosurg* 1997;87:525–534.
33. Speck O, Thiel T, Hennig J. Grading and therapy monitoring of astrocytomas with $^1$H-spectroscopy: Preliminary study. *Anticancer Res* 1996;16:1581–1585.
34. Tedeschi G, Lundbom N, Raman R, *et al.* Increased choline signal coinciding with malignant degeneration of cerebral gliomas: A serial proton magnetic resonance spectroscopy imaging study. *J Neurosurg* 1997;87:516–524.
35. Behar KL, den Hollander JA, Stromski ME, *et al.* High-resolution $^1$H nuclear magnetic resonance study of cerebral hypoxia in vivo. *Proc Natl Acad Sci USA* 1983;80:4945–4948.
36. Schwickert G, Walenta S, Sundfor K, Rofstad EK, Mueller-Klieser W. Correlation of high lactate levels in human cervical cancer with incidence of metastasis. *Cancer Res* 1995;55: 4757–4759.
37. Walenta S, Salameh A, Lyng H, *et al.* Correlation of high lactate levels in head and neck tumors with incidence of metastasis. *Am J Pathol* 1997;150:409–415.
38. Bhujwalla ZM, Glickson JD. Detection of tumor response to radiation therapy by in vivo proton MR spectroscopy. *Int J Radiat Oncol Biol Phys* 1996;36:635–639.
39. Mahmood U, Alfieri AA, Thaler H, Cowburn D, Koutcher JA. Radiation dose-dependent changes in tumor metabolism measured by $^{31}$P nuclear magnetic resonance spectroscopy. *Cancer Res* 1994;54:4885–4891.
40. Street JC, Mahmood U, Matei C, Koutcher JA. In vivo and in vitro studies of cyclophosphamide chemotherapy in a mouse mammary carcinoma by $^{31}$P NMR spectroscopy. *NMR Biomed* 1995;8:149–158.
41. Freyer JP. Phosphomonoesters and growth fraction in multicellular spheroids. Baltimore, MD: International Society of Magnetic Resonance in Medicine, Johns Hopkins University; Aug. 8–9, 1996.
42. Freyer JP, Schor PL, Jarrett KA, Neeman M, Sillerud LO. Cellular energetics measured by phosphorous nuclear magnetic resonance spectroscopy are not correlated with chronic nutrient deficiency in multicellular tumor spheroids. *Cancer Res* 1991;51:3831–3837.
43. Gillies RJ, Barry JA, Ross BD. In vitro and in vivo $^{13}$C and $^{31}$P NMR analyses of phosphocholine metabolism in rat glioma cells. *Magnetic Reson Med* 1994;32:310–318.
44. Dewhirst MW, Sostman HD, Leopold KA, *et al.* Soft-tissue sarcomas: MR imaging and MR spectroscopy for prognosis and therapy monitoring. Work in progress. *Radiology* 1990; 174(3 Pt 1):847–853.
45. Prescott DM, Charles HC, Sostman HD, *et al.* Therapy monitoring in human and canine soft tissue sarcomas using magnetic resonance imaging and spectroscopy. *Int J Radiat Oncol Biol Phys* 1994;28:415–423.
46. Brizel DM, Scully SP, Harrelson JM, *et al.* Radiation therapy and hyperthermia improve the oxygenation of human soft tissue sarcomas. *Cancer Res* 1996;56:5347–5350.
47. Scheidhauer K, Scharl A, Pietrzyk U, *et al.* Qualitative [$^{18}$F]FDG positron emission tomography in primary breast cancer: Clinical relevance and practicability. *Eur J Nuclear Med* 1996;23:618–623.
48. Rigo P, Paulus P, Kaschten BJ, *et al.* Oncological applications of positron emission tomography with fluorine-18 fluorodeoxyglucose. *Eur J Nuclear Med* 1996;23:1641–1674.
49. Utech CI, Young CS, Winter PF. Prospective evaluation of fluorine-18 fluorodeoxyglucose positron emission tomography in breast cancer for staging of the axilla related to surgery and immunocytochemistry. *Eur J Nuclear Med* 1996;23:1588–1593.
50. Avril N, Bense S, Ziegler SI, *et al.* Breast imaging with fluorine-18-FDG PET: Quantitative image analysis. *J Nuclear Med* 1997;38:1186–1191.
51. Brock CS, Meikle SR, Price P. Does fluorine-18 fluorodeoxyglucose metabolic imaging of tumours benefit oncology? [see comments]. *Eur J Nuclear Med* 1997;24:691–705.
52. Kiffer JD, Berlangieri SU, Scott AM, *et al.* The contribution of $^{18}$F-fluoro-2-deoxy-glucose positron emission tomographic imaging to radiotherapy planning in lung cancer. *Lung Cancer* 1998;19:167–77.
53. Munley MT, Marks LB, Scarfone C, *et al.* Multimodality nuclear medicine imaging in three-dimensional radiation treatment planning for lung cancer: Challenges and prospects. *Lung Cancer* 1999;23:105–114.
54. Haberkorn U, Strauss LG, Dimitrakopoulou A, *et al.* PET studies of fluorodeoxyglucose metabolism in patients with recurrent colorectal tumors receiving radiotherapy. *J Nuclear Med* 1991;32:1485–1490.
55. Minn H, Lapela M, Klemi PJ, *et al.* Prediction of survival with fluorine-18-fluoro-deoxyglucose and PET in head and neck cancer. *J Nuclear Med* 1997;38:1907–1911.
56. Fischman AJ, Thornton AF, Frosch MP, Swearinger B, Gonzalez RG, Alpert NM. FDG hypermetabolism associated with inflammatory necrotic changes following radiation of meningioma. *J Nuclear Med* 1997;38:1027–1029.
57. Tjuvalev JG, Macapinlac HA, Daghighian F, *et al.* Imaging of brain tumor proliferative activity with iodine-131-iododeoxyuridine. *J Nuclear Med* 1994;35:1407–1417.
58. Shields AF, Mankoff DA, Graham MM, *et al.* Monitoring tumor response to chemotherapy with [C-11]-thymidine and FDG PET. *J Nuclear Med* 1998;37:290–296.

59. Shields AF, Mankoff DA, Link JM, *et al.* Carbon-11-thymidine and FDG to measure therapy response. *J Nuclear Med* 1998;39:1757–1762.
60. Hara T, Kosaka N, Kishi H. PET imaging of prostate cancer using carbon-11-choline. *J Nuclear Med* 1998;39:990–995.
61. Thomlinson RH, Gray LH. The histological structure of some human lung cancers and the possible implications for radiotherapy. *Br J Cancer* 1955;9:539–549.
62. Overgaard J, Horsman MR. Modification of hypoxia-induced radioresistance in tumors by the use of oxygen and sensitizers. *Semin Radiat Oncol* 1996;6:10–21.
63. Hockel M, Schlenger K, Mitze M, Schaffer U, Vaupel P. Hypoxia and radiation response in human tumors. *Semin Radiat Oncol* 1996;6:3–9.
64. Brizel DM, Scully SP, Harrelson JM, *et al.* Tumor oxygenation predicts for the likelihood of distant metastases in human soft tissue sarcoma. *Cancer Res* 1996;56:941–943.
65. Hockel M, Schlenger K, Aral B, Mitze M, Schaffer U, Vaupel P. Association between tumor hypoxia and malignant progression in advanced cancer of the uterine cervix. *Cancer Res* 1996;56:4509–4515.
66. Rasey JS, Koh WJ, Evans ML, *et al.* Quantifying regional hypoxia in human tumors with positron emission tomography of [$^{18}$F]fluoromisonidazole: A pretherapy study of 37 patients. *Int J Radiat Oncol Biol Phys* 1996;36:417–428.
67. Chapman JD, Engelhardt EL, Stobbe CC, Schneider RF, Hanks GE. Measuring hypoxia and predicting tumor radioresistance with nuclear medicine assays. *Radiother Oncol* 1998; 46:229–237.
68. Blankenberg F, Katsikis P, Tait J, *et al.* In vivo detection and imaging of phosphatidylserine expression during programmed cell death. *Proc Natl Acad Sci USA* 1998;95:6349–6354.
69. Vriens P, Blankenberg F, Stoot J, *et al.* The use of technetium Tc 99m Annexin V for in vivo imaging of apoptosis during cardiac allograft rejection. *J Thorac Cardiovasc Surg* 1998; 116:844–853.
70. Tjuvajev JG, Finn R, Watanabe K, *et al.* Noninvasive imaging of herpes virus thymidine kinase gene transfer and expression: A potential method for monitoring clinical gene therapy. *Cancer Res* 1996;56:4087–4095.
71. Larson SM, Tjuvajev J, Blasberg R. Triumph over mischance: A role for nuclear medicine in gene therapy [editorial; comment] [see comments]. *J Nuclear Med* 1997;38:1230–1233.
72. Rogers BE, Rosenfeld ME, Khazaeli MB, *et al.* Localization of iodine-125-mIP-Des-Met14-bombesin (7–13)$NH_2$ in ovarian carcinoma induced to express the gastrin releasing peptide receptor by adenoviral vector-mediated gene transfer [see comments]. *J Nuclear Med* 1997;38:1221–1229.
73. Nunez MI, McMillan TJ, Valenzuela MT, Ruiz de Almodovar JM, Pedraza V. Relationship between DNA damage, rejoining and cell killing by radiation in mammalian cells. *Radiother Oncol* 1996;39:155–165.
74. Li GC, Ouyang H, Li X, *et al.* Ku70: A candidate tumor suppressor gene for murine T cell lymphoma. *Molec Cell* 1998;2:1–8.
75. Ling CC, Endlich B. Radioresistance induced by oncogenic transformation. *Radiat Res* 1989;120:267–279.
76. McKenna WG, Weiss MC, Endlich B, *et al.* Synergistic effect of the V-myc oncogene with H-ras on radioresistance. *Cancer Res* 1990;50:97–102.
77. Bristow RG, Benchimol S, Hill RP. The p53 gene as a modifier of intrinsic radiosensitivity: Implications for radiotherapy. *Radiother Oncol* 1996;40:197–223.
78. Brown JM, Wouters BG. Apoptosis, p53 and tumor cell sensitivity to anticancer agents. *Cancer Res* 1999;59:1391–1399.
79. Austin-Seymour M, Chen GT, Rosenman J, Michalski J, Lindsley K, Goitein M. Tumor and target delineation: Current research and future challenges. *Int J Radiat Oncol Biol Phys* 1995;33:1041–1052.
80. Raleigh JA, Dewhirst MW, Thrall DE. Measuring tumor hypoxia. *Semin Radiat Oncol* 1996;6:37–45.